Proceedings of the ASME 2013 Fluids Engineering Summer Meeting
FEDSM2013
July 7-11, 2013, Incline Village, Nevada, USA

FEDSM2013-16479

SHARP INTERFACE CAVITATION MODELING USING VOLUME-OF-FLUID AND LEVEL SET METHODS

Thad Michael
Carderock Division
Naval Surface Warfare Center
Bethesda, Maryland, USA

Jianming Yang
IIHR - Hydroscience & Engineering
University of Iowa
Iowa City, Iowa, USA

Frederick Stern
IIHR - Hydroscience & Engineering
University of Iowa
Iowa City, Iowa, USA

ABSTRACT

A sharp interface cavitation modeling methodology is presented. A simplified Rayleigh-Plesset equation is used to obtain the phase change rate from the local pressure. The phase change rate is expressed as mass flux jump conditions. The phase interface is tracked using a second-order volume-of-fluid method with a constructed level set function. The interface normal velocity jump is extended into the flow field using a fast marching method. A ghost fluid method is used to prevent difficulties computing high-order derivatives near the interface. Two separate intermediate velocity fields from the momentum equation are solved considering the velocity jump conditions. Some preliminary results will be demonstrated to show the promise of the present approach.

INTRODUCTION

Cavitation occurs when a liquid, such as water, changes state to a vapor due to a reduction in pressure. For example the flow around a lifting surface such as a hydrofoil or propeller blade causes a low pressure on the suction side.

Cavitation reduces the lift produced by these surfaces and the collapse of cavitation bubbles may cause physical damage to the surface. When cavitation cannot be prevented, it is important to be able to accurately model the effects of cavitation.

Cavitation modeling consists of two parts: the modeling of multiphase flow and the modeling of the mass transfer between the phases. In this work, a coupled level set and volume-of-fluid sharp interface method is used for the multiphase model. A new method is developed for modeling the mass transfer with a sharp interface model. The new method is implemented in CFDShip-IOWA Version 6 (Yang and Stern, 2009).

Previous cavitation modeling efforts include both potential flow models and models applicable to finite volume and finite difference methods.

This paper reviews the physics of cavitation and past simulation efforts. Then, the details of the model used in this paper are presented, followed by examples with a single bubble and a hydrofoil with cavitation. A parametric investigation of the effect of the vapor pressure and constants for evaporation and condensation was made to determine the effects of the parameters. The effect of the vapor viscosity was also investigated.

NOMENCLATURE

c	chord length of foil
C_p	pressure coefficient, $p/\rho u^2$
F	volume-of-fluid scalar
$\boldsymbol{g}$	gravity vector
$\dot{m}$	mass flux between phases
$\boldsymbol{n}$	normal vector
p	pressure
p_{vap}	vapor pressure at ambient temperature
R	radius
t	time
$\boldsymbol{u}$	velocity vector
$\boldsymbol{U}$	interface velocity vector
x	streamwise direction
y	cross-stream direction
ρ	density

Subscripts

f	fluid
l	liquid
N	normal
v	vapor

BACKGROUND

Cavitation is the term for the change of state of a liquid to a vapor caused by a low pressure region within a flow field. In contrast, the term boiling is used when a fluid changes from liquid to vapor due to a high temperature. Both are similar phenomena and have the same physical mechanisms—

in both cases the liquid reaches a combination of pressure and temperature that dictate a change of state to vapor. In cavitation, the local pressure drops below the vapor pressure at the ambient temperature. In boiling, the vapor pressure at the local temperature rises above the ambient pressure. Therefore, in the case of boiling, the surrounding heat flux is critical while the local pressure is relatively unimportant, whereas in cavitation the heat flux is relatively unimportant but the pressure field is critical.

Potential flow cavitation models have been successfully applied to propellers by Lee (1979) and Kerwin *et al.* (1987). These models use lifting surface theory or potential panels to represent the blade surface. Cavities are modeled with sources or additional panels.

Many researchers have explored cavitation modeling with finite volume and finite difference codes using homogenous mixture models. Phase change models for use with the mixture model were developed by Merkle *et al.* (1998) and Kunz, *et al.* (1999) and are still commonly used. A slightly more recent model by Singhal *et al.* (2002) is based on similar principles and adds the ability to model non-condensable gas within the bubbles. Recent computations by Kim *et al.* (2008, 2010a, 2010b) and Bensow *et al.* (2008) using these models, or similar ones, have shown good comparison with hydrofoil and propeller experiments.

In contrast to homogenous mixture models, sharp interface models subdivide computational cells into a liquid part and a vapor part. This reduces diffusion due to advection.

Sharp interface models for phase change have been demonstrated for the case of film boiling by Son and Dhir (2007) and Gibou *et al.* (2007). The research described in this paper applies related techniques to the problem of cavitation. The application of the volume source and interface velocity jump is similar. However, cavitation may be a more difficult problem than boiling because of the tight coupling between the pressure solution and the phase change rate which is not present in boiling problems.

MATHEMATICAL MODEL

Navier-Stokes equations

The incompressible viscous flow of the liquid and vapor are governed by the Navier-Stokes equations

$$\nabla \boldsymbol{u} = 0 \tag{1}$$

$$\frac{\partial \boldsymbol{u}}{\partial t} + \boldsymbol{u} \cdot \nabla \boldsymbol{u} = \frac{1}{\rho} \nabla \cdot (-p\boldsymbol{I} + \boldsymbol{T}) + \boldsymbol{g} \tag{2}$$

where $\boldsymbol{I}$ is the identity matrix and

$$\boldsymbol{T} = 2\mu \boldsymbol{S} \tag{3}$$

where μ is the viscosity of the fluid and

$$\boldsymbol{S} = \frac{1}{2}[\nabla \boldsymbol{u} + (\nabla \boldsymbol{u})^T] \tag{4}$$

Jump Conditions

The well-known Rankine-Hugoniot jump conditions are required to satisfy mass and momentum conservation at the interface.

$$\left[\rho_f \left(\boldsymbol{u}_{f_N} - \boldsymbol{U}_N\right)\right] = 0 \tag{5}$$

$$\left[\rho_f \left(\boldsymbol{u}_{f_N} - \boldsymbol{U}_N\right)^2 + p\right] = 0 \tag{6}$$

where $\boldsymbol{u}_{f_N}$ and $\boldsymbol{U}_N$ are the normal components of the fluid and interface velocities, respectively, and $[X]$ denotes the jump in quantity X across the interface. The mass flux between phases is

$$\dot{m} = \rho_l(\boldsymbol{U}_N - \boldsymbol{u}_{l_N}) = \rho_v(\boldsymbol{U}_N - \boldsymbol{u}_{v_N}) \tag{7}$$

This also satisfies the mass conservation requirement that the mass flux from one phase is balanced by the mass flux to the other phase

$$[\dot{m}] = 0 \tag{8}$$

Interface Tracking

The interface is tracked with the sharp volume-of-fluid (VOF) method with a constructed distance function as described by Wang *et al.* (2012). The method is modified to use the interface velocity described in the preceding section.

The interface represents the boundary between liquid and vapor. However particles cross the interface when changing phases. This model accounts for the change in the location of the interface as a thin slice of fluid at the interface is converted from one phase to the other.

The VOF advection equation without phase change is

$$\frac{\partial F}{\partial t} + \boldsymbol{u}\nabla F = 0 \tag{9}$$

When phase change is included, the VOF is advected by the interface velocity, $\boldsymbol{U}$, so that

$$\frac{\partial F}{\partial t} + \boldsymbol{U}\nabla F = 0 \tag{10}$$

With mass transfer between phases, the interface velocity is the combination of the fluid velocity, $\boldsymbol{u}_f$, and the relative velocity due to phase change such that

$$\boldsymbol{U} = \boldsymbol{u}_f + \frac{\dot{m}\boldsymbol{n}}{\rho_f} \tag{11}$$

The effect of phase change can be visualized with the example of water evaporating from a glass. The liquid velocity is zero. But, as molecules of liquid become vapor at the surface, the interface moves downward with the velocity described by Equation 11.

The Mass Flux Model

Phase change models for cavitation can be divided into three broad categories: barotropic models, equilibrium models, and Rayleigh-Plesset based models. Barotropic models simply define all fluid above vapor pressure as liquid and all fluid below vapor pressure as vapor. Equilibrium models seek to accurately compute the phase change rate determined by the heat transfer from liquid to vapor, but require very small time steps due to the high rate of conduction through liquid water and the small gradient near the interface. Rayleigh-Plesset models simplify the physics by utilizing a simplification of the Rayleigh-Plesset equation for bubble dynamics; this has the potential to capture the most significant aspects of the physics without requiring exceedingly small time steps. The models commonly in use with the homogenous mixture model are derived from the Rayleigh-Plesset equation.

Franc and Michel (2004) showed that the rate of heat transfer in water is sufficiently high that it can be neglected for most practical problems. The Rayleigh-Plesset equation describes the evolution of a three-dimensional, spherical bubble filled with saturated vapor and subject to uniform pressure variations.

$$\rho_l\left(R\ddot{R}+\frac{3}{2}(\dot{R}^2)\right) = p_{vap}-p_\infty+p_{g0}\left(\frac{R_0}{R}\right)^{3\gamma}-\frac{2S}{R}-4\mu\frac{\dot{R}}{R} \tag{12}$$

where p_{g0} is the initial partial pressure of non-condensable gasses, R_0 is the initial radius of the bubble, S is the surface tension, and γ is the ratio of the gas heat capacities. The third term on the right hand side represents the effect of the non-condensable gasses. The last two terms on the right represent the effects of surface tension and viscosity, respectively. The surface tension can be neglected for all but the smallest bubbles and the viscous effects can be neglected for the Reynolds numbers of interest in ship flows.

If we note that the time-varying term on the left of Equation 12 can be expressed

$$R\ddot{R}+\frac{3}{2}\dot{R}^2=\frac{1}{2\dot{R}R^2}\frac{d\left(\dot{R}^2R^3\right)}{dt} \tag{13}$$

Then, dropping the non-condensable gas, surface tension, and viscosity terms and integrating with respect to time yields

$$\frac{dR}{dt}=\sqrt{\frac{2}{3}\frac{(p_\infty-p_{vap})}{\rho_l}\left(1-\left(\frac{R_0}{R}\right)^3\right)} \tag{14}$$

The cube of the initial radius, R_0, represents the volume of non-condensable gasses present in the nuclei before phase change caused the bubble to grow. Hence, the ratio of the initial radius to the instantaneous radius of a cavitation bubble will be small once cavitation growth begins until just before bubble collapse, both below the expected resolution of the flow solver. Therefore, the cube of the ratio can be neglected, leaving

$$\frac{dR}{dt}=\sqrt{\frac{2}{3}\frac{(p_\infty-p_{vap})}{\rho_l}} \tag{15}$$

This equation describing the time rate of change of a bubble radius subject to a pressure field is the foundation of several mass-transfer phase-change models where the local pressure replaces the far field pressure in the equation above.

In the volume-of-fluid and level set methods, bubbles must be larger than a cell to be tracked. When the interface is convected in the volume-of-fluid method, it is modeled as a plane in each cell. If the radius is sufficiently large, then the rate of change of the radius with respect to time can be approximated by the advancement of the planar interface in the direction normal to the interface during a time step. That is, the phase change velocity can be approximated as

$$\frac{\dot{m}\boldsymbol{n}}{\rho_l}=\sqrt{\frac{2}{3}\frac{(p-p_{vap})}{\rho_l}}\,\boldsymbol{n} \tag{16}$$

so that

$$\dot{m}=\sqrt{\frac{2}{3}\rho_l(p-p_{vap})} \tag{17}$$

Since the local pressure must be used in place of the far field pressure, a constant is added for correlation. As in models by Merkle *et al.* (1998) and Singhal *et al.* (2002), different constants may be used for evaporation and condensation.

$$\dot{m}=\begin{cases}C_e\sqrt{\frac{2}{3}\rho_l(p_{vap}-p)}, & p<p_{vap}\\ C_c\sqrt{\frac{2}{3}\rho_l(p-p_{vap})}, & p\geq p_{vap}\end{cases} \tag{18}$$

where C_e and C_c are the evaporation and condensation coefficients, respectively.

NUMERICAL MODEL

Discretization

The governing equations are discretized on a non-uniform staggered orthogonal curvilinear grid, with the velocity components defined at the centers of the cell faces and all other variables defined at the cell centers. A finite difference approach is used, with the exception of the pressure Poisson equation, where a finite volume approach is used for increased stability. Additional details can be found in Suh e*t al.* (2011).

The pressure Poisson equation with phase change is

$$\frac{\partial}{\partial x_i} Grad_i(p^{n+1}) = \frac{1}{\Delta t}\left(\frac{\partial u_i^*}{\partial x_i} + \dot{m}\left(\frac{1}{\rho_v} - \frac{1}{\rho_l}\right)\right) \tag{19}$$

where the term on the far right represents the volume source due to phase change. $Grad_i(p)$ is collocated with the velocity components and incorporates the jump conditions due to surface tension and gravity as described by Yang and Stern (2009). A first-order Euler method is used for time advancement for simplicity.

Volume of Fluid and Level Set

The VOF-PLIC scheme presented by Gueyffier *et al*. (1999) is employed for the interface reconstruction. After the interface is reconstructed, the VOF fluxes can be calculated and the interface is propagated by updating the VOF values in the entire computational domain. The interface is reconstructed on the computational domain rather than on the physical domain. The interface is advected separately in each coordinate direction using an operator splitting strategy. In the first fractional step, the normal vector is calculated from the level set function of the previous time step; then the intermediate level set function is used to calculate the normal vector in the second fractional step. Further description of the method can be found in Wang *et al.* (2012).

The level set function is reinitialized from the VOF using a fast marching method (Yang and Stern, 2011). The level set function is used for convenience in determining interface distances and normals and computed in conjunction with extending the velocity jump at the interface throughout the domain for use in the ghost fluid method, described later.

Velocity Jump

The velocity jump is treated in an integral fashion, consistent with the finite volume approach to the Poisson equation. This is done by considering a flux jump due to the phase change which results in a jump in the average velocity at cell faces. It is not necessary for the interface to separate two velocity points. The ratio of the area of the interface in a given direction to the mean area of the cell faces in that direction is used to modify the expected velocity jump.

$$[\boldsymbol{u}] = \dot{m}\left[\frac{1}{\rho}\right]\frac{A_f}{A_i}\,\boldsymbol{n} \tag{20}$$

where A_f is the face area and A_i is the interface area. The interface area is determined from the VOF volume fraction by finding the points where the interface intersects the cell edges, as described by Wang *et al.* (2012). The area is then computed by a series of cross-products between the interface edge vectors.

With this method, source terms slowly increase and decrease in a cell as the interface moves through the cell. If a cell has a volume fraction between zero and one, then it will contain a volume source contributing a flux jump proportional to the interface area and normal component in each direction.

Ghost Fluid Method

The ghost fluid method was introduced by Fedkiw *et al*. (1999) for multiphase compressible flows without phase change and extended by Nguyen *et al*. (2001) to incompressible flame fronts with mass transfer. The method was employed by Son and Dhir (2007) and Gibou *et al*. (2007) using the level set method to compute boiling problems.

The momentum solver used in this research includes the effects of surface tension and the density and viscosity changes between the fluid fields (Yang and Stern 2009). Therefore, the ghost fluid method is only applied to the normal velocity jump due to phase change.

To extend the liquid velocity field, the jump in normal velocity is removed from cells in the vapor region by applying

$$\boldsymbol{u}_l = \boldsymbol{u}_v - \dot{m}\left[\frac{1}{\rho}\right]\boldsymbol{n} \tag{21}$$

at cells where the volume fraction is equal to zero, therefore all vapor. To determine the value of $\dot{m}$ away from the interface, the level set fast marching method developed by Yang and Stern (2011) has been modified to simultaneously extend the value of $\dot{m}$ at the interface in the normal direction, following the method described by Herrmann (2003).

The vapor velocity field is extended in a similar fashion. The intermediate velocity fields are predicted separately, then the two fields are recombined using the phase indicated by the level set function.

Semi-Implicit Phase Change Rate

For stability, the pressure Poisson equation is modified to include the phase change equation semi-implicitly. To do this, the source term is linearized and separated into implicit and explicit parts.

$$\dot{m}\left(\frac{1}{\rho_v} - \frac{1}{\rho_l}\right) = sign(p - p_{vap})E\sqrt{|p - p_{vap}|} \tag{22}$$

where E is the constant

$$E = \left(\frac{1}{\rho_v} - \frac{1}{\rho_l}\right)\sqrt{\frac{2}{3}\rho_l} \tag{23}$$

The square root is linearized similar to Kim and Brewton (2008):

$$sign(p - p_{vap})\sqrt{|p^{n+1} - p_{vap}|} = \frac{p^{n+1} - p_{vap}}{\sqrt{|p^n - p_{vap}|}} \tag{24}$$

Now, the source term can be represented by semi-implicit and explicit parts:

$$\dot{m}\left(\frac{1}{\rho_v} - \frac{1}{\rho_l}\right) = \frac{E\,p^{n+1}}{\sqrt{|p^n - p_{vap}|}} - \frac{E\,p_{vap}}{\sqrt{|p^n - p_{vap}|}} \tag{25}$$

The revised pressure Poisson equation is

$$\frac{\partial}{\partial x_i} Grad_i(p^{n+1}) - \frac{E\, p^{n+1}}{\sqrt{|p^n - p_{vap}|}} = \frac{1}{\Delta t}\left(\frac{\partial u_i^*}{\partial x_i} - \frac{E\, p_{vap}}{\sqrt{|p^n - p_{vap}|}}\right) \quad (26)$$

which determines the mass flux between phases simultaneously with the solution of the pressure Poisson equation.

When the pressure and vapor pressure are equal, the denominator of both the explicit and semi-implicit terms will be zero. This is consistent with the infinite slope of the phase change rate at this point. To manage this situation, a minimum denominator is selected. A minimum denominator of 0.5 provides first derivative continuity.

The contribution of the pressure jump due to momentum conservation is much smaller than the volume source. An explicit method has been tested, to evaluate the magnitude of the term, but has not been included in these results for simplicity.

VERIFICATION

To test the implementation of the volume source and jump conditions, a simple two-dimensional bubble of radius one is computed on a round mesh with a specified volume source strength corresponding to

$$\dot{m} = \frac{0.1}{R}\left(\frac{1}{\rho_v} - \frac{1}{\rho_l}\right) \quad (27)$$

The ratio of the density of liquid to the density of vapor is 1000. The bubble is expanding with the source strength inversely proportional to the bubble radius. Consequently, the velocity field outside of the bubble will be constant in time. The outer boundary pressure is fixed at zero, so that the pressure near the bubble, where the velocity is greater, must be lower.

For these conditions, the analytical solution of the velocity and pressure field is known. Figure 1 compares the computed radial pressure distribution with the analytical solution for a point source. The symbols show the analytical solution while the lines show the computed solution for the first 50 time steps. In the bubble case, the source is initially at the interface at r=1 so that the velocity inside the bubble is zero and the pressure is constant in space. As time advances, the radius of the bubble increases and the pressure in the bubble increases to match the analytical value at the current interface radius.

To test the semi-implicit phase change computation and two dimensions, an expanding bubble with an initial radius of one is computed on a square mesh with dimensions of -10 to 10 in each direction and 512 cells in each direction, with cells clustered in way of the bubble. The far field pressure is zero and the vapor pressure is two. Since the ambient pressure is below vapor pressure, the bubble will grow.

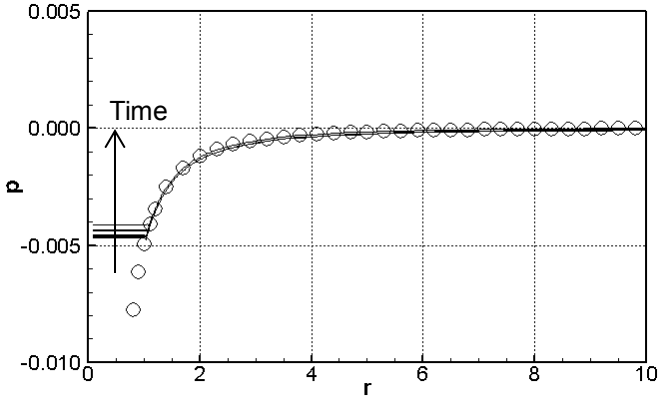

Figure 1: Comparison of computed and analytical solutions for bubble pressure field.

Initially, the velocity is zero everywhere. During the first time step, the implicit phase change model allows pressure in the bubble to rise almost to vapor pressure, to accelerate liquid away from the bubble. In subsequent time steps, the velocity near the bubble increases and the pressure near the bubble is reduced, as shown in Figure 2. The time step size is 0.01; the first 20 time steps, 25, 30, and 40 are shown. The bubble grows slowly at this point, and the change in radius from 1.00 to 1.03 is not clearly visible in the figure.

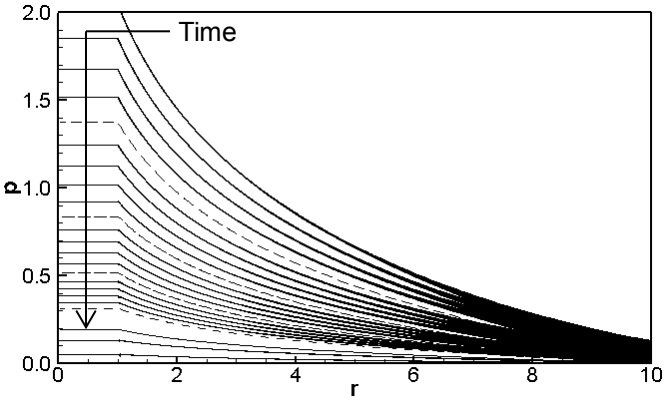

Figure 2: Expanding bubble on a square mesh with computed phase change rate.

Figure 3 shows velocity vectors and pressures for a small part of the interface at time step 30. There are some variations in the pressure due to discretization. The velocity vectors outside of the bubble clearly point outward and the vectors inside of the bubble are near zero, clearly showing the velocity jump produced by the volume source at the interface. Equation 11 indicates that the interface is moving into the liquid at a slightly higher rate than the liquid is moving outward as a thin slice of liquid is converted to a larger volume of vapor to make the new outer ring of the expanding bubble.

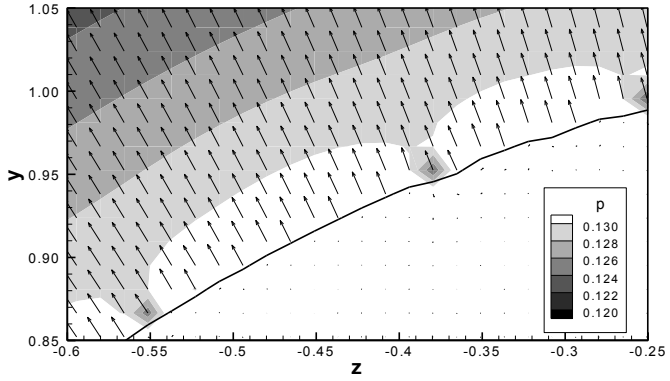

Figure 3: Velocity vectors and pressure at the interface.

RESULTS AND DISCUSSION

A NACA66 hydrofoil with 2% camber and 9% thickness described by Shen and Dimotakis (1989) was computed in two dimensions on an O-grid of 256×2048 cells with a radius of about 10 chord lengths. An inlet velocity boundary condition was used upstream and a fixed pressure boundary condition was used downstream. Figure 4 shows the geometry and Figure 5 shows the mesh near the leading edge.

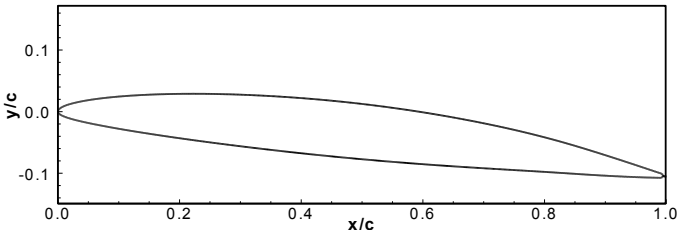

Figure 4: NACA 66 hydrofoil at six-degree angle of attack.

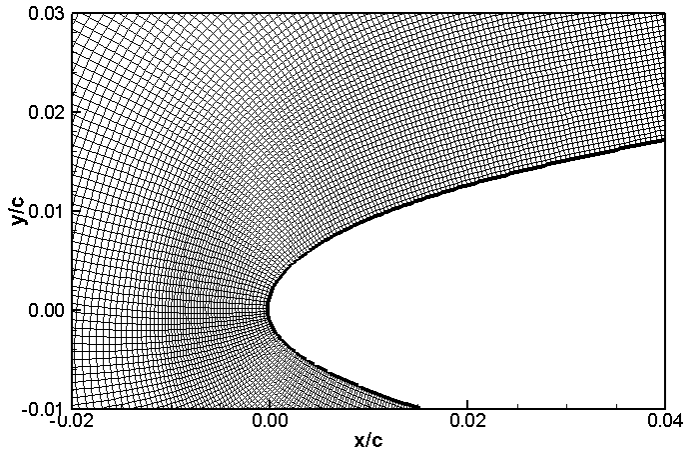

Figure 5: Grid at leading edge of the foil.

Figure 6 compares the non-cavitating pressure distribution with the experimental measurements at a six-degree angle of attack. Note that the figure shows the negative pressure coefficient, so that the pressure on the suction side of the foil appears on top. The far field pressure is zero.

Figure 7 compares the cavities at pressure coefficients of -0.50, -0.45, and -0.40 at the same time step. As expected when the far field pressure is closer to the vapor pressure there is more cavitation. When bubbles are shed downstream, they maintain the pressure at the interface at close to vapor pressure as they shrink to prevent any pressure increase. In these figures, the coefficient for evaporation is 3.5 and the coefficient for condensation is 1.0. The low pressure "spot" is a bubble which has shrunk below the resolution of the level set function.

Figure 8 shows the evolution of the cavitation at a vapor pressure coefficient of -0.50 starting at the time step shown in Figure 7. The cavity sheds bubbles downstream in a repeating cycle.

The evaporation coefficient is important for maintaining the position of the cavity near the leading edge of the hydrofoil. The leading edge of the cavity will travel downstream if the rate of evaporation is insufficient to counteract advection. Evaporation constants of three to four were found to be sufficient to maintain the position of the leading edge of the cavity.

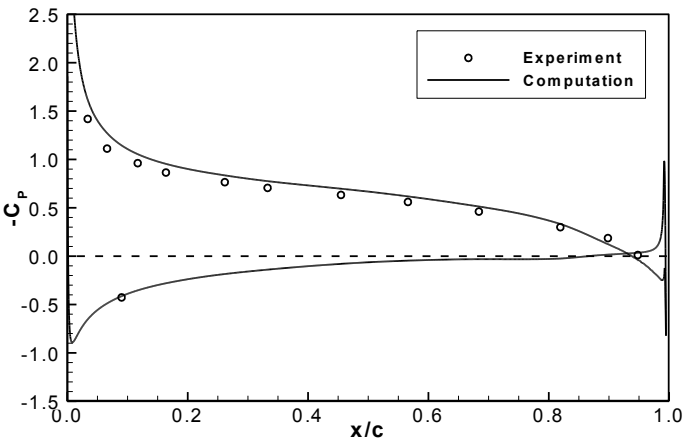

Figure 6: Non-cavitating pressure distribution at six-degree angle of attack.

The rate of condensation is important for determining the length of the cavity, and how long bubbles persist after they are shed downstream. It was found that a lower rate of condensation than evaporation was desirable, as in the model developed by Singhal (2002). However, if the rate of condensation is too low, the bubbles will be slow to contract and travel far downstream.

Figure 9 compares condensation rate coefficients of 0.1, 1.0, and 2.0 at a vapor pressure coefficient of -0.50. The figure shows that with a condensation coefficient of 0.1 the shed bubbles persist, shrinking very slowly in comparison to the higher values. The large bubble near x/c=0.55 at the lowest

condensation coefficient eventually travels past the trailing edge of the foil.

The viscosity of the vapor has some effect on the shedding of the cavities through its presence in the momentum equation. Figure 10 compares results with ratios of vapor dynamic viscosities to liquid dynamic viscosities of 0.1 and 0.01 at the same time step with a vapor pressure coefficient of -0.50. At room temperature, the ratio of the water vapor viscosity to the liquid water viscosity is about 0.01 while the ratio of air viscosity to liquid water viscosity is 0.10. The smaller vapor viscosity results in smaller leading edge cavities and more frequent shedding.

CONCLUSIONS

A sharp interface model for cavitation has been developed. The model utilizes a simplification of the Rayleigh-Plesset equation to determine the rate of phase change. This rate is computed semi-implicitly as part of the solution of the pressure Poisson equation where the phase change rate acts as a volume source. The rate of phase change is used directly to determine the velocity of the sharp interface.

Initial results show that the implementation of the volume source and ghost fluid method result in a pressure field that matches the analytical value for a specified phase change rate.

Wetted results with a NACA 66 hydrofoil show that the computed wetted pressure distribution is in good agreement with the measurements. Initial parametric results for cavitating conditions show the correct physics and much detail at the interface. The importance of selecting the correct coefficients for condensation and evaporation is clear. The coefficients will be selected by comparison with experiments. Future work will compare the cavitating computations with experimental measurements. Currently, no subgrid model for bubbles has been implemented. Such a model will be needed to more accurately model the creation and destruction of bubbles.

ACKNOWLEDGMENTS

T. Michael's time at the University of Iowa has been supported by the US Department of Defense SMART Program and by the NSWCCD Carderock Division ILIR Program, which is funded by the Office of Naval Research. F. Stern and J. Yang were sponsored by the US Office of Naval Research through research grant N000141-01-00-1-7 under the administration of Dr. Patrick Purtell.

The simulations presented in this paper were performed at the Department of Defense (DoD) Supercomputing Resource Centers (DSRCs) through the High Performance Computing Modernization Program (HPCMP).

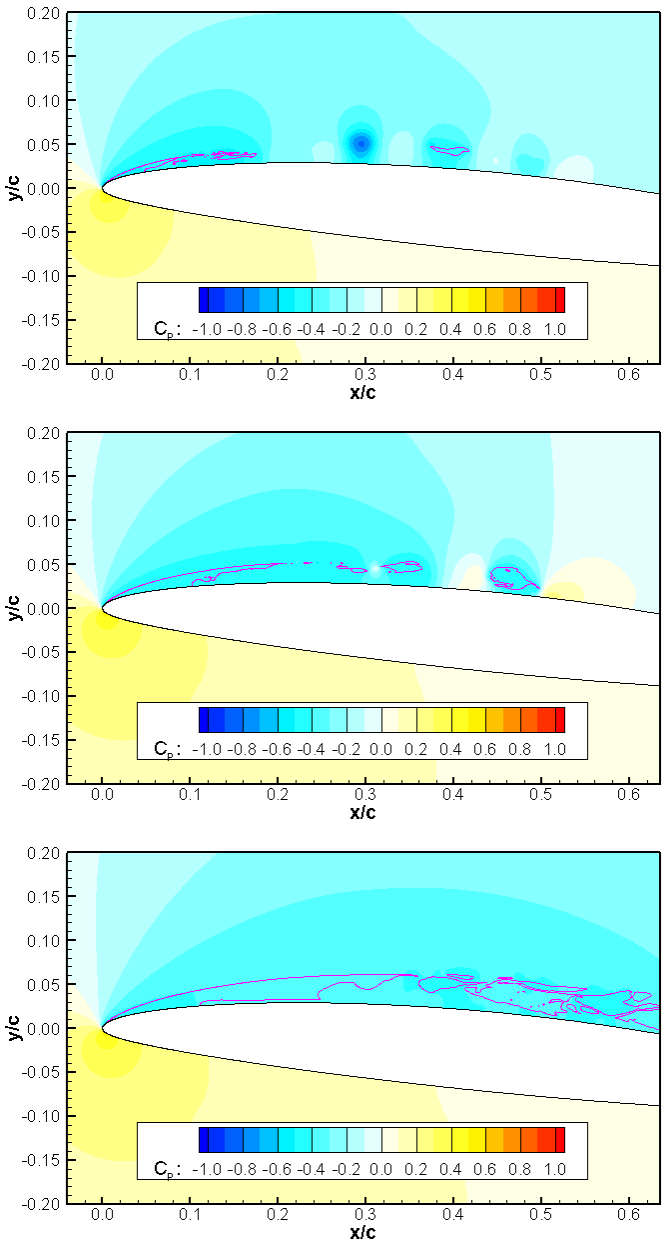

Figure 7: Cavitation with vapor pressure coefficients of -0.50, -0.45, -0.40 (top to bottom).

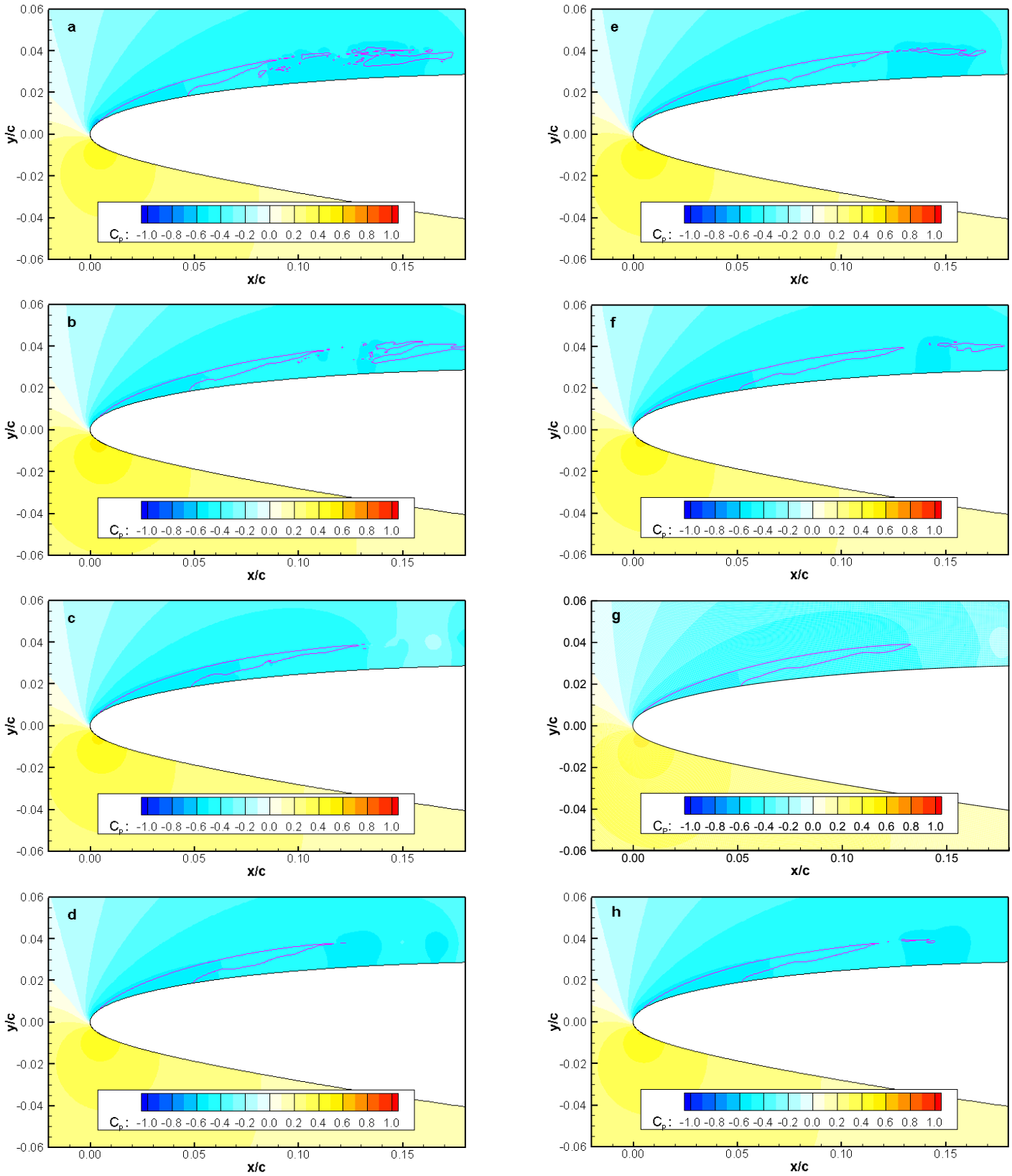

Figure 8: Evolution of the leading edge cavity with C_{Pvap}=-0.50, time advancing a-h

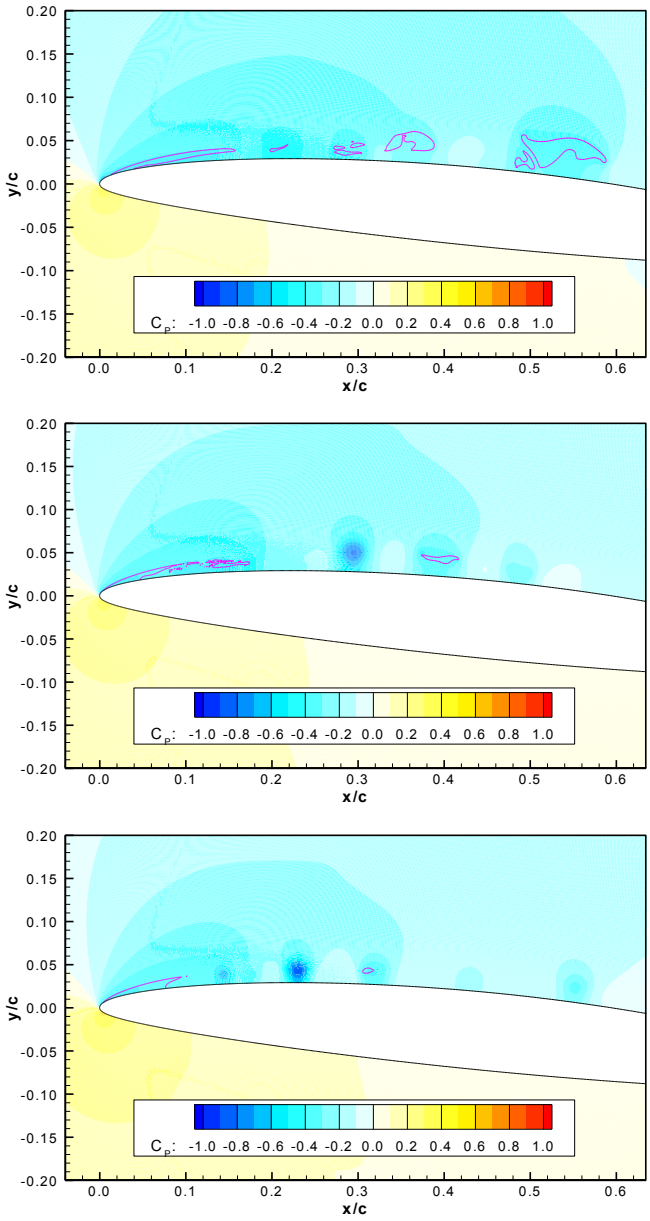

Figure 9: Varying condensation coefficient 0.1, 1.0, 2.0 (top to bottom), with C_{Pvap}=-0.50.

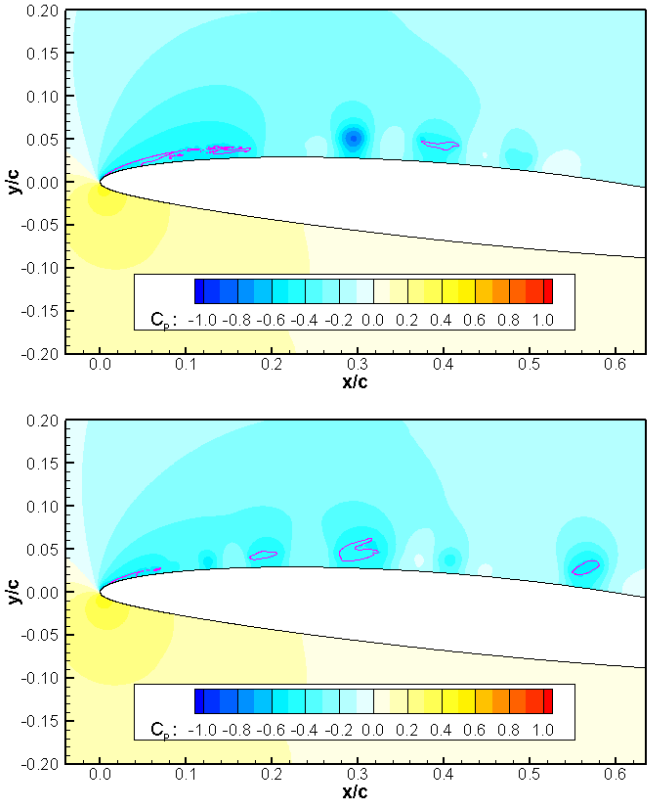

Figure 10: Effect of vapor dynamic viscosity ratio, 0.10 (top) and 0.01 (bottom) with C_{Pvap}=-0.50.

REFERENCES

Bensow, R.E., T. Huuva and G. Bark. 2008. Large eddy simulation of cavitating propeller flows. 27th Symposium on Naval Hydrodynamics, 5-10 October, Seoul, Korea.

Franc, J.-P. and J.-M. Michel. 2004. *Fundamentals of Cavitation*. Dordracht: Kluwer Academic Publishers.

Gibou, F., L. Chen, D. Nguyen, and S. Banerjee. 2007. A level set based sharp interface method for the multiphase incompressible Navier-Stokes equations with phase change. *Journal of Computational Physics*, 222:536-555.

D. Gueyffier, J. Li, A. Nadim, R. Scardovelli, S. Zaleski. 1999. Volume-of-fluid interface tracking with smoothed surface stress methods for three-dimensional flows. *J. Comput. Phys,* 152:423–456.

Fedkiw, R.P., T. Aslam, B. Merriman, and S. Osher. 1999. A non-oscillatory Eulerian approach to interfaces in multimaterial flows (the ghost fluid method). *Journal of Computational Physics*, 152:457-492.

Herrmann, M. 2003. A domain decomposition parallelization of the fast marching method. *Center for Turbulence Research Annual Research Briefs*, 213-225.

Kerwin, J.E. , S.A. Kinnas, J.-T. Lee, and W.-Z. Shih. 1987. A surface panel method for the hydrodynamic analysis of ducted propellers. *SNAME Transactions*, 95:93-122.

Kim, S.-E. and S. Brewton. 2008. A multiphase approach to turbulent cavitating flows. Proceedings of the 27th Symposium on Naval Hydrodynamics, Seoul, Korea, October 5-10.

Kim, S.-E., S. Schroeder and H. Jasak. 2010a. A multi-phase CFD framework for predicting performance of marine propulsors. The 13th International Symposium on Transport Phenomena and Dynamics of Rotating Machinery, April 4-7, Honolulu, Hawaii, USA.

Kim, S.-E. and S. Schroeder. 2010b. Numerical study of thrust-breakdown due to cavitation on a hydrofoil, a propeller, and a waterjet. *Proceedings of the 28th Symposium on Naval Hydrodynamics*, 12-17 September, Pasedena, California, USA.

Kunz, R.F., D.A. Boger, T.S. Chyczewski, D.R. Stinebring, and H.J. Gibeling. 1999. Multi-phase CFD analysis of natural and ventilated cavitation about submerged bodies. Proceedings of FEDSM ’99, 3rd ASME/JSME Joint Fluids Engineering Conference, July 18-23, San Francisco, California, USA.

Lee, C.-S. 1979. *Prediction of steady and unsteady performance of marine propellers with or without cavitation by numerical lifting surface theory*. PhD dissertation, Massachusetts Institute of Technology, Cambridge, Massachusetts, USA.

Merkle, C. L., J.Z. Feng and P.E.O. Buelow. 1998. Computational modeling of the dynamics of sheet cavitation. Third International Symposium on Cavitation, April 7-10, Grenoble, France.

Nguyen, D.Q., R.P. Fedkiw, and M. Kang. 2001. A boundary condition capturing method foriIncompressible flame discontinuities. *Journal of Computational Physics*. 172:71-98.

Shen, Y.T. and P.E. Dimotakis. 1989. The influence of surface cavitation on hydrodynamic forces. 22nd American Towing Tank Conference, August 8-11, St Johns, Newfoundland, Canada.

Singhal, A.K., M.M. Athavale, H. Li, and Y. Jiang. 2002. Mathematical basis and validation of the full cavitation model. *Journal of Fluids Engineering*. 124:617-624.

Son, G. and V.K. Dhir. 2007. A level set method for analysis of film boiling on an immersed solid surface. *Numerical Heat Transfer, Part B: Fundamentals*, 52: 153-177.

Suh, J., J. Yang, and F. Stern. 2011. The effect of air-water interface on the vortex shedding from a vertical circular cylinder. *Journal of Fluids and Structures*, 27:1-22.

Wang, Z., J. Yang, and F. Stern. 2012. A new volume-of-fluid method with a constructed distance function on general structured grids. *Journal of Computational Physics*, 231:3703-3722.

Yang, J. and F. Stern. 2009. Sharp interface immersed-boundary/level-set method for wave-body interactions. *Journal of Computational Physics*, 228:6590-6616.

Yang, J. and F. Stern. 2011. A simple and efficient parallel implementation of the fast marching method. The 64th Annual Meeting of the American Physical Society - Division of Fluid Dynamics, Baltimore, Maryland, USA.